Dalton Transactions

Large Magnetic Anisotropy of a Decorated Spin-Chain System K2Co3(MoO4)3(OH)2

Journal:	*Dalton Transactions*
Manuscript ID	DT-ART-01-2024-000203.R1
Article Type:	Paper
Date Submitted by the Author:	10-Feb-2024
Complete List of Authors:	Patel, Bhakti; Clemson University, Chemistry Ye, Feng; Oak Ridge National Laboratory, Material Sciences Liyanage, Namila; The University of Tennessee Knoxville, Department of Physics and Astronomy Buchanan, Charlotte; The University of Tennessee Knoxville, Materials Science and Engineering Gilbert, Dustin; University of Tennessee Knoxville College of Engineering, Material Science and Engineering and Physics & Astronomy Kolis, Joseph; Clemson University, Chemsitry Sanjeewa, Duminda; University of Missouri System, Chemistry; MURR

Large Magnetic Anisotropy of a Decorated Spin-Chain System $K_2Co_3(MoO_4)_3(OH)_2$

Bhakti K. Patel,[a] Feng Ye,[b] W. L. N. C. Liyanage,[c] C. Charlotte Buchanan,[d] Dustin A. Gilbert,[c,d] Joseph W. Kolis,[a] Liurukara D Sanjeewa[e,f*]

[a]*Department of Chemistry and Center for Optical Materials Science and Engineering Technologies (COMSET), Clemson University, Clemson, SC 29634-0973, USA*
[b]*Neutron Scattering Division, Oak Ridge National Laboratory, Oak Ridge, TN 37831, USA*
[c]*Department of Physics and Astronomy, University of Tennessee, Knoxville, Tennessee 37996, USA*
[d]*Materials Science and Engineering, University of Tennessee, Knoxville, Tennessee 37996, USA*
[e]*University of Missouri Research Reactor (MURR), University of Missouri, Columbia, MO 65211, USA*
[f]*Department of Chemistry, University of Missouri, Columbia, MO 65211, USA*

**Corresponding Author*

Abstract

The magnetic structure of $K_2Co_3(MoO_4)_3(OH)_2$ is studied in detail. The material has a half-sawtooth one-dimensional (1-D) structure containing two unique Co^{2+} ions, one in the chain backbone and one on the apex of the sawtooth creating a series of isosceles triangles along the *b*-axis. These triangles can be a source of magnetic frustration. The ability to grow large single crystals enables detailed magnetic measurements with the crystals oriented in a magnetic field along the respective axes. It has a Curie-Weiss temperature θ_{CW} of 5.3(2) K with an effective magnetic moment of 4.8(3) μ_B/Co. The material is highly anisotropic with a sharp antiferromagnetic ordering transition at 7 K with a metamagnetic transition at 2 kOe. Neutron diffraction was used to determine the magnetic structure and revealed a magnetic structure with canted spins along the backbone of the chain while spins along the sawtooth caps maintained a colinear orientation, arranging antiferromagnetically relative to the backbone spins. The parallel chains arrange antiferromagnetically relative to each other along the *c*-axis and ferromagnetically along the *a*- axis.

1. Introduction

The study of novel quantum materials is one of the most exciting aspects of modern materials science, and relies on correlating the atomic structure and the magnetic lattice to determine the fundamental physical properties.[1-3] The synergy between materials chemistry and condensed matter physics continues to stimulate the discovery of new materials with complex magnetic properties. Magnetic materials with a geometrically frustrated triangular lattice have garnered significant interest among these two scientific communities since they hold great potential to find quantum spin liquid (QSL) candidates. These could be the key to future quantum based applications such as quantum communication and computation.[4-5] Two-dimensional (2-D) materials with geometrical constraints, such as triangular, honeycomb, and Kagome lattices, are the most studied candidates for quantum spin liquid behavior.[6-9] Several other systems including numerous complex triangular 2-D and one-dimensional (1-D) chains have been investigated. Among these exotic materials, 2-D magnetic lattices including stripe Kagome and triangular stripe layers, and 1-D triangular spin chains such as sawtooth chains, half sawtooth chains, and triangular spin tubes are of particular interest because of their intriguing magnetic properties.[13-18] Competition between first, second, and third nearest neighbor magnetic exchange interactions often leads to rich magnetic phase diagrams of these materials. Moreover, these materials provide a platform to study the effect of the change of lattice dimensionality with different arrangements of the basic triangular magnetic building unit.[19-20]

Among these materials, sawtooth and half sawtooth chains represent special classes of triangular 1-D compounds.[14-17] The sawtooth magnetic lattice is comprised of corner-sharing triangles pointing alternately in opposite directions in a sawtooth fashion along a 1-D chain, while in half-sawtooth chains these triangles sit on only one side of the 1-D chain.[14] Experimental realization of

sawtooth and half-sawtooth lattice structures is scarce, but we recently made excellent progress in synthesizing these materials using a high-pressure high-temperature hydrothermal method.[14-17] Using this method, large single crystals can be grown that are suited not only to collect detailed anisotropic magnetic measurements, but also to perform single crystal neutron diffraction, thereby allowing a detailed understanding of the fundamental magnetic properties of these materials.[21-23] A further advantage of hydrothermally grown single crystals is that their structural defects are minimized by the lower temperatures and solution-based synthesis method, which is extremely important in understanding the fundamental physical properties of these compounds.[24-25] In this context, the use of tetrahedral oxyanion ($[AsO_4]^{3-}$, $[MoO_4]^{2-}$, $[VO_4]^{3-}$) chemistry is an excellent route to achieve novel 1-D materials.[14,16,22] These non-magnetic oxyanion building blocks can isolate the transition metal magnetic chains, minimizing the interchain interactions. They have become a fertile ground to investigate novel quantum phenomena in low dimensional magnetic materials because of these properties. We are investigating the magnetic properties of arsenate ($[AsO_4]^{3-}$), molybdate ($[MoO_4]^{2-}$), and selenite [$(SeO_3)^{2-}$] based transition metal sawtooth compounds, which display a considerable range of unusual magnetic properties.[14-16] Moreover, these oxyanion-based structures also retain a wide range of structural flexibility by adopting overall 1-D, 2-D and three-dimensional (3-D) crystal structures.[24-25]

Oxyanion-based sawtooth lattices $Rb_2Fe_2O(AsO_4)_2$, $CsCo_2(MoO_4)_2(OH)$ and $NaCo_2(SeO_3)_2(OH)$ exhibit complex and highly anisotropic magnetic properties.[14-16] On the other hand, the sawtooth structure euchroite-cuprate $Cu_2(AsO_4)(OH)$ does not show any long-range magnetic ordering down to milli-K temperatures, suggesting a magnetic frustration due to the competing interactions in the frustrated $S = 1/2$ magnetic lattice.[26] So far, $Rb_2Mn_3(MoO_4)_3(OH)_2$ and

$K_2Mn_3O(OH)(VO_4)(V_2O_7)$ are the only candidates available as the half-sawtooth lattice.[17,27] $Rb_2Mn_3(MoO_4)_3(OH)_2$ exhibits a complex magnetic phase diagram with two consecutive magnetic transitions, including a transition from a paramagnetic to an incommensurate phase below 4.5 K and a commensurate antiferromagnetic (AFM) transition below 3.5 K, which have been previously confirmed by single crystal neutron diffraction.[17] $K_2Mn_3O(OH)(VO_4)(V_2O_7)$ is a unique half-sawtooth chain structure made from edged-sharing $Mn^{2+}O_6$ and $Mn^{3+}O_6$ octahedra which undergoes an antiferromagnetic transition at T_N = 14.4 K. The unique magnetic properties of these compounds showcase the potential for exploiting novel magnetic materials that will pave the way for greater fundamental understanding of 1-D triangular spin chain systems.

In this work, we report on the magnetic properties of the half-sawtooth $K_2Co_3(MoO_4)_3(OH)_2$ single crystals synthesized by a high temperature hydrothermal method. $K_2Co_3(MoO_4)_3(OH)_2$ crystals exhibit a pronounced anisotropic magnetic susceptibility and isothermal magnetization along the Co–O–Co half-sawtooth chain direction (*b*-axis). The compound undergoes long range ordering at 7 K and isothermal magnetization data confirms the presence of a field induced transition at relatively low applied magnetic field (H < 2 kOe, H//*b*-axis). The magnetic structure was investigated using single crystal neutron diffraction. Magnetic structure refinement reveals ferromagnetic (FM) configuration along the Co−O−Co chain, and antiparallel arrangement between the chains, resulting in an overall antiferromagnetic (AFM) ordering.

2. Experimental Section

Single crystals of $K_2Co_3(MoO_4)_3(OH)_2$ were grown using the high-temperature high-pressure hydrothermal method. A detailed hydrothermal synthesis and single crystals structure

characterization is given in Ref 28. The typical size of the single crystals is 0.5 × 1 × 2.5 mm^3. Single crystal X-ray diffraction also used to confirm the orientation of the single crystals, with the long axis of the crystals being the *b*-axis of the unit cell. The structural parameters determined from single crystal X-ray diffraction at room temperature are given in the supporting information. Table 1 displays the select bond distances and bond angles of $K_2Co_3(MoO_4)_3(OH)_2$.

Magnetic properties were determined using one single crystal with a mass of 6.8 mg. Magnetometry measurements were performed using a vibrating sample magnetometer attached to the Quantum Design Dynacool PPMS. Both temperature and field dependent magnetization data were collected with the applied magnetic field along the crystallographic directions, *a*-, *b*- and *c*-axis, respectively. The *b*-axis is the Co−O−Co chain direction as displayed in Figure 2 inset. Temperature dependent magnetic measurements were collected from 350 to 2.5 K with the applied magnetic field ranging from 100 Oe to 50 kOe. Isothermal magnetization data were collected up to 50 kOe from 2.5 to 100 K.

Single-crystal neutron diffraction experiments were carried out using CORELLI spectrometer at the Spallation Neutron Source (SNS) using a 20 mg single crystal. CORELLI is a quasi-Laue time-of-flight instrument with an incident neutron wavelength band between 0.7 Å and 2.9 Å. It has a large 2-D detector array, with a −30˚ to +150˚ in-plane coverage and ±28˚ out-of-plane coverage.[29-30] The sample was mounted horizontally on the (0*kl*) plane and the vertical rotation axis is along the *a*-axis. Experiments were conducted by rotating the sample for ≈360 ˚ with a 3˚ step at base temperatures of 100 , 15 and 1.5 K. Bragg peaks collected at 1.5 K were used for the refinement with total of 20900 Bragg reflections. The temperature dependence of the (3,1,0) magnetic

diffraction peak was measured between 1.5 and 15 K to extract a magnetic ordering parameter. The MANTID package was used for data reduction.[31] The neutron diffraction data were analyzed by using the Jana2020 and FullProf Suite Package and the magnetic space group was determined using the MAXMAGN program in Bilbao Crystallographic Server.[32-35]

Table 1. Selected bond lengths and bond angles of $K_2Co_3(MoO_4)_3(OH)_2$ obtained from the single crystal Xray diffraction. The refined single crystal Xray diffraction data: orthorhombic, *Pnma* (No. 62), a = 17.9394(4) Å, b = 6.0836(2) Å, c = 12.3969(4) Å, V = 1352.95 Å^3.

Co(1)O$_6$		**Co(2)O$_6$**	
Co(1)–O(1)	2.002(3) Å	Co(2)–O(1)	2.009(2) Å
Co(1)–O(4) × 2	2.149(2) Å	Co(2)–O(2)	1.963(2) Å
Co(1)–O(6) × 2	2.211(2) Å	Co(2)–O(3)	2.156(2) Å
Co(1)–O(9)	1.957(3) Å	Co(2)–O(5)	2.121(2) Å
		Co(2)–O(6)	2.318(2) Å
		Co(2)–O(8)	2.121(2) Å
Co(1)–O(1)–Co(2)	107.05˚	Co(2)–O(1)–Co(2)	99.45˚
Co(1)–O(6)–Co(2)	90.83˚	Co(2)–O(2)–Co(2)	100.44˚
Co(2)–O(8)–Co(2)	92.61(2)˚	Co(2)–O(3)–Co(2)	88.78˚
J_1 via O(1), O(8) Co(2)–Co(2) = 3.067(2) Å			
J_2 via O(2), O(3) Co(2)–Co(2) = 3.017(2) Å			
J_3 via O(1), O(6) Co(1)–Co(2) = 3.226(2) Å			

3. Results

3.1. Crystal structure of $K_2Co_3(MoO_4)_3(OH)_2$

$K_2Co_3(MoO_4)_3(OH)_2$ crystallizes in orthorhombic crystal system space group *Pnma* (No. 62) with unit cell parameters of a = 17.9394(4) Å, b = 6.0836(2) Å, c = 12.3969(4) Å, and a resulting unit cell volume of V = 1352.95 Å^3, and with Z = 4. $K_2Co_3(MoO_4)_3(OH)_2$ and $Rb_2Mn_3(MoO_4)_3(OH)_2$ are iso-structures. A detailed discussion about the structure of $K_2Co_3(MoO_4)_3(OH)_2$ is given in Ref 28, therefore the description given below focuses on the structure in the context of the magnetic

properties. A picture of a hydrothermally grown, columnar-shaped single crystal is given in Figure 1a. The projected view of the $K_2Co_3(MoO_4)_3(OH)_2$ structure along the *b*-axis shows the connectivity between Co–O–Co half-sawtooth chains and the molybdate groups (Figure 1b). The system is comprised of two unique crystallographic Co-sites: Co(1) located in 8*d* with Wyckoff position of (0.40172(1), 0.25, 0.25767(6)) and Co(2) at 4*c* site (0.55509(5), 0.50205(4), 0.31399(6)). The edge-sharing, distorted CoO_6-octahedra form Co–O–Co triangular chain structures along the *b*-axis (Figure 1c). These chains are interconnected via $[MoO_4]^{2-}$ groups to form a three-dimensional structure. The Co(1) atoms sit at the apex of the triangle while the Co(2) atoms form the base of the triangle (Figure 1c). The Co–O bond distances of $Co(1)O_6$ octahedra range from 1.957(3) Å to 2.211(2) Å and those of $Co(2)O_6$ octahedra range from 1.963(2) to 2.318(2) Å, respectively, highlighting the distorted nature of the CoO_6 octahedron. In the Co–O–Co chains one $Co(1)O_6$ shares edges with two $Co(2)O_6$ octahedra via O(1) and O(6) forming the $[Co_3O_{11}]$ triangular units. The Co(1)–O(1)–Co(2) and Co(1)–O(6)–Co(2) bond angles are 107.05˚ and 90.83˚, respectively. Within the $[Co_3O_{11}]$ triangular units, O(3) shares the center between the $Co(1)O_6$ and two $Co(2)O_6$ octahedron units. Moreover, each $[Co_3O_{11}]$ triangular unit interconnects with two more $[Co_3O_{11}]$ triangular units in each side via a $Co(2)O_6$ unit by sharing edges with O(3) and O(2) to form the half-sawtooth chain along the *b*-axis. The Co(2)–O(2)–Co(2) and Co(2)–O(3)–Co(2) bond angles are 100.44˚ and 88.78˚, respectively. There are three different nearest neighbor interactions within the Co–O–Co chains: J_1 (Co(2)–Co(2) = 3.067(2) Å); J_2 (Co(2)–Co(2) = 3.017(2) Å); J_3 (Co(1)–Co(2) = 3.226(2) Å). Since Mo^{6+} is nonmagnetic, the $[MoO_4]^{2-}$ groups minimize direct exchange between the Co–O–Co chains of triangles. However, the distance between the Co–O–Co chains is approximately ≈6.5 Å allowing for additional *interchain* magnetic interactions. In spite of the fact that $K_2Co_3(MoO_4)_3(OH)_2$ and

$Rb_2Mn_3(MoO_4)_3(OH)_2$ are structurally identical, the different spin values (S = 3/2 and S = 5/2 on Mn vs. Co, respectively) and as well as subtle structural differences result in very different magnetic properties. A notable difference between the structures is the distance between the transition metal centers of the half-sawtooth chains. In $Rb_2Mn_3(MoO_4)_3(OH)_2$, the Mn–Mn distances are larger than the Co–Co distances in $K_2Co_3(MoO_4)_3(OH)_2$, partially due to the presence of the larger Rb^+ ions. Also, the Shannon crystal radii is larger for high-spin Mn^{2+} than Co^{2+}, at 0.970 Å and 0.885 Å, respectively.[36] These two factors result in a larger unit cell and longer bond distances in $Rb_2Mn_3(MoO_4)_3(OH)_2$. For example, the average Co–O and Mn–O distances are 2.113(2) and 2.196(2) Å for $K_2Co_3(MoO_4)_3(OH)_2$ and $Rb_2Mn_3(MoO_4)_3(OH)_2$, respectively. A similar behavior is observed with regard to the interchain distances (≈6.5 and ≈6.8 Å) for K- and Rb-based half-sawtooth compounds. Thus $K_2Co_3(MoO_4)_3(OH)_2$ has a more compact structure which could increase the strength of the magnetic interactions and enhance the magnetic anisotropy.

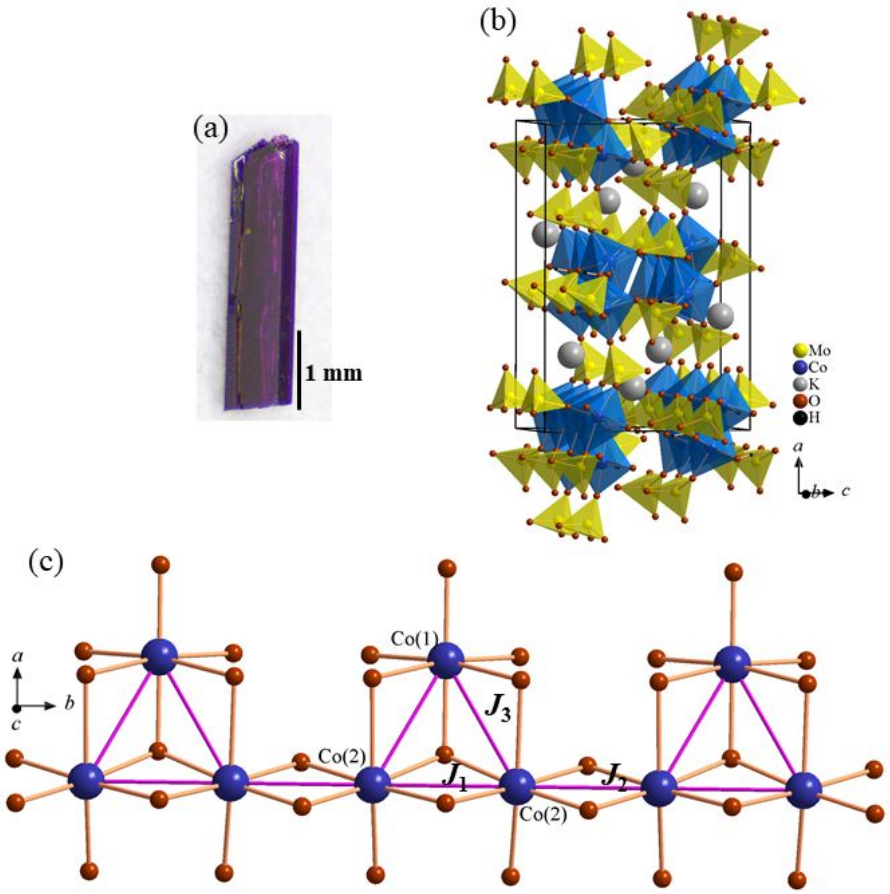

Figure 1. (a) Hydrothermally grown single crystals of $K_2Co_3(MoO_4)_3(OH)_2$. (b) Partial polyhedral view of $K_2Co_3(MoO_4)_3(OH)_2$ projected along the *b*-axis, showing packing of Co–O–Co half-sawtooth chains in the structure. The K^+ ions reside inside the cavities made by CoO_6 octahedron and MoO_4 tetrahedron. (c) Partial structure of Co–O–Co half-sawtooth chains made from edge-sharing CoO_6 octahedra along the *b*-axis. The unequal J_1, J_2 and J_3 exchange interactions are shown using the solid pink line. The Co(2)–Co(2), J_1, Co(2)–Co(2), J_2, Co(1)–Co(2), J_3, distances are 3.067(2), 3.017(2) and 3.226(2) Å, respectively.

3.2 Magnetic Properties of $K_2Co_3(MoO_4)_3(OH)_2$

The magnetic properties of $K_2Co_3(MoO_4)_3(OH)_2$ were examined using the magnetic susceptibility and the isothermal magnetization with the magnetic field oriented along the three crystallographic axes. Figure 2 displays the temperature dependent magnetic susceptibility from 2 - 100 K, measured while cooling in a 500 Oe magnetic field. Magnetic susceptibility in all three directions exhibits a sharp rise below 20 K and a peak at around T_N = 7 K, which is in agreement with the expected Néel temperature, followed by a rapid decrease with lowering temperature. There is a

significant anisotropy between the crystallographic orientations especially at the transition temperature. Here, the magnitude of the magnetic susceptibility is thirty times larger when the magnetic field is along the Co–O–Co chain direction (*b*-axis, easy axis) compared to the other two directions. Figure 2 inset shows the Curie-Weiss fit for the data along the *b*-axis from 150 - 350 K yielding θ_{CW} of 5.3(2) K and an effective magnetic moment of 4.8(3) μ_B/Co. The positive θ_{CW} suggests an overall ferromagnetic interaction along the Co–O–Co chain direction even though the magnetic susceptibility behavior indicates AFM-like behavior at the phase transition. Magnetic susceptibility along the *a*- and *c*-axis is not strictly linear due to the very weak signal because of the highly anisotropic nature of the system. Curie-Weiss fits of the susceptibility measured along the *a*- and *c*-axis produces similar effective magnetic moments, 4.5(2) and 4.6(3) μ_B/Co, respectively (Supporting Information). However, the θ_{CW} values are significantly different, -49.2(3) and -85.0(2) K along the *a*- and *c*-axis, respectively. A similar situation has been observed in other anisotropic 1-D systems such as Sr*M*(VO_4)(OH), *M* = Co and Ni, $BaCo_2V_2O_8$, $CoGeO_3$ and CoV_2O_6.[19,37-40] For example, in the SrCo(VO_4)(OH) system Curie-Weiss fits along the *a*- (easy axis), *b*- and *c*-axis revealed θ_{CW} values of 8, -47 and -181 K, respectively.[22] The higher effective magnetic moment of Co^{2+} versus the ideal spin only values ($S = 3/2$, $\mu_{eff} = 3.8\ \mu_B$) is likely due to the unquenched orbital moment in Co^{2+} in a distorted octahedral environment. Similar situations are very common for Co-based 1-D and 2-D triangular compounds.[40-44] Figure 3a depicts the field dependent magnetic data at 2.5 K along different crystallographic directions, which shows a large magnetic anisotropy between the three axes. When the magnetic field along the Co–O–Co chain direction (*b*-axis) the magnetization indicates a sudden jump at, H_c = 2.0 kOe, indicating a field induced magnetic transition. Comparatively, field induced transitions were observed at much higher fields along the *a*- and *c*-axis, at 20 and 17.5 kOe, respectively. This suggests that the Co

spins produce a ferromagnetic state as they rotate toward the *b*-axis. In other words, the two magnetic sublattices of the antiferromagnetic chain (Co(1) and Co(2)) are capable of rotating the magnetic spins along the *b*-axis in a much more favorable manner than along the *a*- and *c*-axes. Further research on the exchange parameters will provide additional insight into this behavior. Figure 3b displays the isothermal magnetization data along the Co–O–Co direction at various temperatures T = 2.5, 5, 10, 15, 20 and 100 K. At 2.5 K the magnetization reaches a saturation of 1.6 μ_B/Co. Above the T_N the step behavior of the magnetization curves vanishes and it adopts a concave shape with a gradual saturation toward 1.6 μ_B/Co.[45] This could be due to the competing AFM and ferromagnetic (FM) interactions of $K_2Co_3(MoO_4)_3(OH)_2$, where at lower temperatures it behaves like an AFM, while sufficiently larger field stabilizes the FM phase even above T_N. Similar behavior has been observed in pyroxene type 1-D structures such as $NaMnGe_2O_6$ and $NaCrSi_2O_6$.[45-46] To further elucidate the field induced transition along the Co–O–Co chain direction, the field dependent magnetic susceptibility was measured from 0.1 to 50 kOe applied magnetic fields below 20 K (Figure 3c). In this case magnetic susceptibilities measured for $H > 1$ kOe exhibit FM behavior by reaching a maximum at 2.5 K with the magnetic transition pushed further towards the lower temperatures, suggesting a gradual development of a new field-induced ferri- or ferromagnetic state.[14] This further supports the isothermal magnetization data observed when the magnetic field is along the chain direction. The overall magnetic properties suggest that the field induced transition could be a spin-flip type magnetic transition along the half-sawtooth chain direction, which at higher field reaches a fully saturated state. We observed a similar behavior in our previous study of the sawtooth system, $CsCo_2(MoO_4)_2(OH)$.[14]

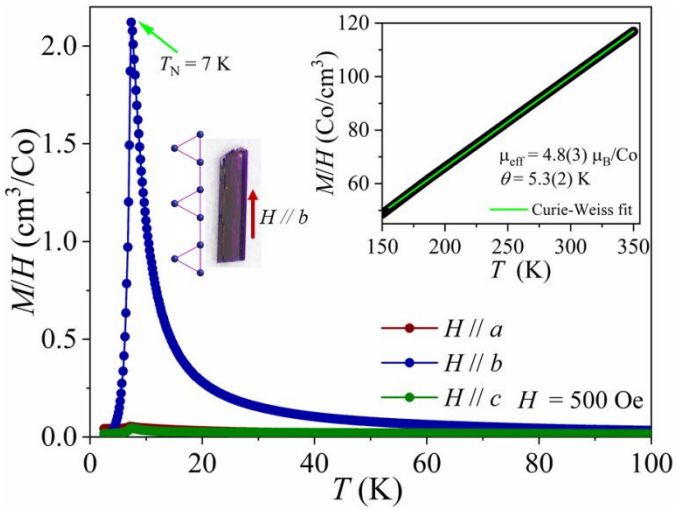

Figure 2. Magnetic susceptibilities, $\chi = M/H$, of $K_2Co_3(MoO_4)_3(OH)_2$ as a function of temperature under an applied field of 500 Oe along the three crystallographic axes. Inset: $K_2Co_3(MoO_4)_3(OH)_2$ crystal highlighting the crystallographic *b*-axis (Co–O–Co chain axis) as the longest axis of the crystals. Temperature dependence of the inverse magnetic susceptibility χ^{-1} in the temperature range 150 K− 350 K. The solid line represents the Curie−Weiss fitting to the data from 150 to 350 K.

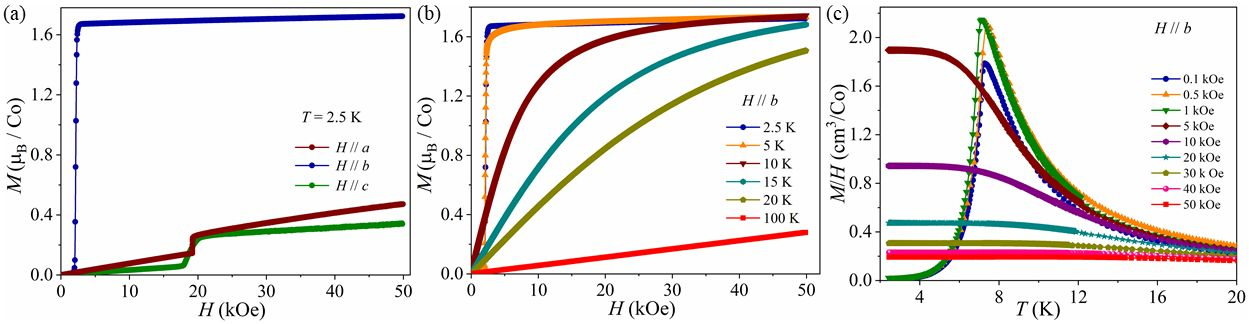

Figure 3. (a) Isothermal magnetization data at 2.5 K along the three crystallographic axes. (b) The isothermal magnetization data along the *b*-axis within the temperature range of 2.5 - 100 K. (c) Field dependent magnetic susceptibility of $K_2Co_3(MoO_4)_3(OH)_2$ measured in different magnetic fields along the *b*-axis (H = 100 Oe – 50 kOe) below 20 K.

3.3 Magnetic Structure of $K_2Co_3(MoO_4)_3(OH)_2$

Single crystal neutron diffraction data were collected at temperatures above and below the magnetic transition. Figures 4a and 4b compare the slice data (HK0) measured at temperatures of 15 and 1.5 K, respectively. In the paramagnetic state, at 15 K, strong nuclear Bragg peaks appear

at H = 2*n* positions (Figure 4a). Comparing to the diffraction pattern below the magnetic transition, at 1.5 K, no additional forbidden peaks violating the reflection condition of the paramagnetic state or superlattice reflections are observed at the magnetic ordered state (Figure 4b). A systematic search for magnetic peaks was performed by subtracting the 15 K data as background from the 1.5 K data. The intensity of the Bragg peaks with odd number of *h* and *k* positions shows considerable enhancement at low temperature. This survey confirms the magnetic propagation vector **k** = (0,0,0), and the magnetic unit cell remains the same as the structural one. The final refinements were carried out using the combined crystal and magnetic intensities from 1.5 K data. The temperature dependence of the integrated intensity of the (3,1,0) peak is shown in Figure 4c. The change of the (3,1,0) peak intensity was fitted using the $I(T) \propto (1\text{-}T/T_N)^{2\beta}$; the fitted profile identifies T_N = 7.3(3) K, in good agreement with the magnetization measurements. The obtained β value is 0.33(2), which is very close to the critical exponent value for the 3-D Ising model (β = 0.3265(3)).[47] A similar Ising critical exponent has recently been reported for the quasi-1-D antiferromagnet *S* = 3/2 $SrCo_2V_2O_8$ system.[48]

Starting from the paramagnetic space group of *Pnma* and the propagation vector **k** = (0,0,0) we used the magnetic space group search available in MAXMAGAN in the Bilbao Crystallographic Server. There are eight possible magnetic space groups available for the *Pnma* space group with a **k** = (0,0,0) propagation vector: *Pnma* (No. 62.441), *Pn'm'a'* (No. 62.449), *Pnm'a'* (No. 62.447), *Pn'ma* (No. 62.443), *Pn'ma'* (No. 62.448), *Pnm'a* (No. 62.444), *Pn'm'a* (No. 62.446) and *Pnma'* (No.62.445). Further refinements were performed based on these possible magnetic space groups. Note that the magnetic susceptibility and isothermal magnetization data confirm that the magnetic moment is predominantly along the *b*-axis and the system is AFM. Therefore, the magnetic space

groups with FM ground state can be easily excluded. The remaining four magnetic space groups have the Co(1) moment only along the *b*-axis and the Co(2) moment allowed in all three directions. Those four magnetic space groups are *Pnma* (No. 62.441), *Pn'ma* (No. 62.443), *Pn'm'a'* (No. 62.449) and *Pnma'* (No.62.445). Among those, the *Pnma'* (No.62.445) refinement agrees well with the experimental data obtained at 1.5 K (Figure 4d).

Figure 5a displays the schematic view of magnetic moments of the Co–O–Co half-sawtooth chain along *b*-axis. According to the model *Pnma'* (No.62.445), within the half-sawtooth chain the Co(1) moment (green arrow) and Co(2) (cyan arrow) moment are paired in opposite direction. The Co(1) moment is constrained along the *b*-axis while Co(2) has a moment along all three crystallographic directions. The Co(2) moment is canted along the *b*-axis and forms an undulating pattern along the half-sawtooth chain direction. This arrangement gives a net moment to the half-sawtooth chain (FM chains along the *b*-axis). Figure 5b shows the coupling of FM half-sawtooth chains within the unit cell along the *ab*-planes; the FM half-sawtooth chains are parallel to each other along the *a*-axis, however the polarity of the FM chains alternates along the *c*-direction creating an overall AFM structure.

The refined magnetic moments of Co(1) and Co(2) are 0.81(3) μ_B (m_a = 0, m_b = 0.81(3) μ_B, m_c = 0)) and 3.81(2) μ_B (m_a = -1.362(1) μ_B, m_b = -3.304(2) μ_B, m_c = 1.594(2) μ_B), respectively. The ordered moment of Co(1) is significantly lower compared to the moment of Co(2) and to the expected moment for spin only Co^{2+} (S = 3/2), μ_{eff} = 3.8 μ_B/Co. This could be due to the different degrees of frustrations of the two Co-sites which are arranged in a triangular fashion in the half - sawtooth chain lattice. The lower moment could also be due to a possible spin-state transition from

S = 3/2 to S = 1/2 (spin crossover) at lower temperatures since Co^{2+} could possess a Kramer's doublet ground state (S_{eff} = ½) in the presence of a crystal electric field and spin-orbital coupling due to the distorted nature of the CoO_6-octahedra; similar magnetic behavior is observed in $Rb_2Fe_2O(AsO_4)_2$, $CsCo_2(MoO_4)_2(OH)$ and $NaCo_2(SeO_3)_2(OH)$ sawtooth structures.[14-17] For example, the refined moments for the two Co sites in $CsCo_2(MoO_4)_2(OH)$ are 1.5 and 3.7 μ_B, respectively. The exact nature for such behavior remains unclear and further theoretical and experimental characterization including inelastic neutron scattering (INS) studies are essential to uncover the underlying microscopic mechanism. Unfortunately no detailed INS studies of sawtooth or half-sawtooth structures have been reported as yet. One may also notice that the magnetic structure of $K_2Co_3(MoO_4)_3(OH)_2$ is different from its sister compound, $Rb_2Mn_3(MoO_4)_2(OH)_2$ where a complicated incommensurate-commensurate magnetic structure was observed. Interestingly, we did not observe two magnetic transitions in either magnetic susceptibility or neutron scattering experiments of $K_2Co_3(MoO_4)_3(OH)_2$ down to 2 K. On the basis of our findings, one can reason that the complexity of the magnetic properties among the saw tooth and half-sawtooth spin chains is quite extensive.

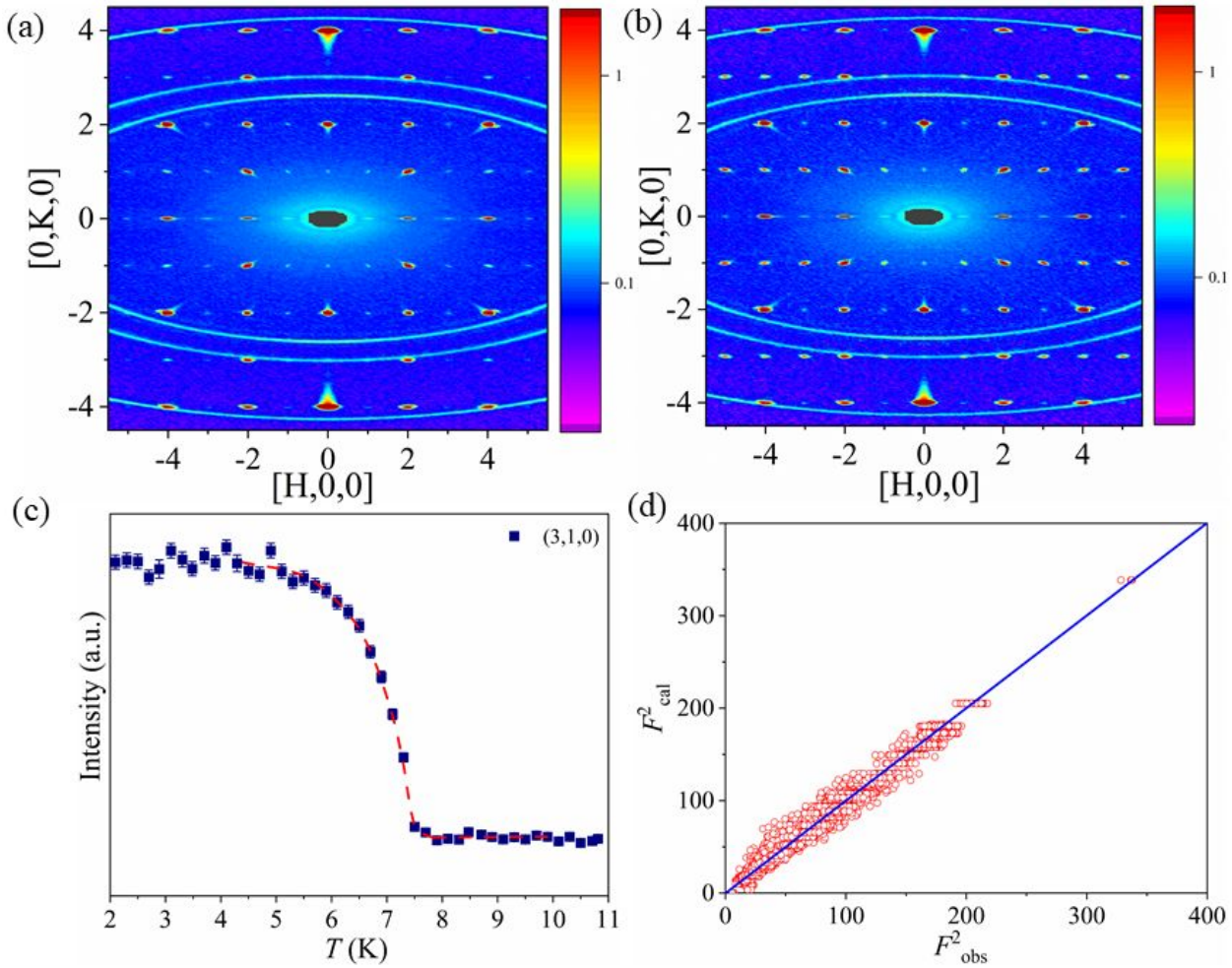

Figure 4. (a) Data for the (HK0) plane at 15 K. (b) Data for the (HK0) plane at 1.5 K. (c) Temperature dependence of the (3,1,0) magnetic peak. (d) Single crystal of $K_2Co_3(MoO_4)_3(OH)_2$ refinement of 1.5 K data showing the observed peak intensities versus the peak intensities of a calculated model.

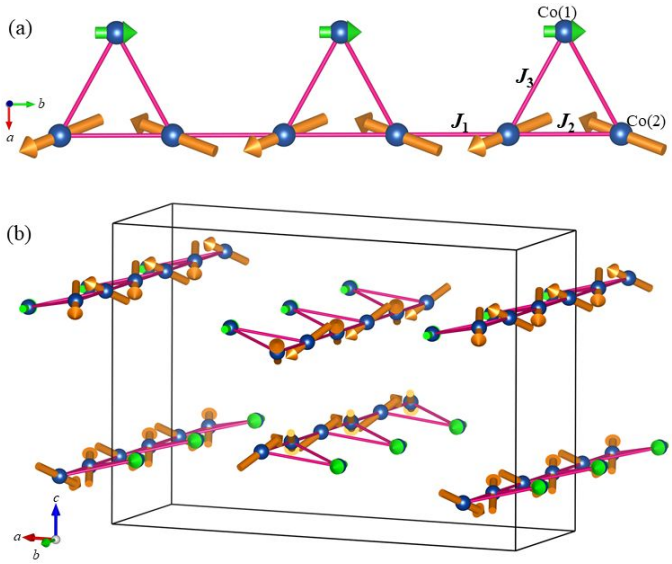

Figure 5. (a) Stereographic view of spin structure of Co–O–Co half-sawtooth chain, the green arrows represent the magnetic moments of Co(1) and cyan arrows represent the Co(2) . The nearest neighbor Co distances are depicted as solid pink lines. (b) Overall magnetic structure at 1.5 K showing the ferromagnetic chains along the *ab*-plane. These planes arrange opposite direction creating a net AFM structure.

4. Conclusions

We continue our investigation of magnetically frustrated 1-D chains of the sawtooth and half-sawtooth class of compounds. Our ability to grow large, high quality single crystals comprised of 1-D chains with sawtooth and half-sawtooth structures, enables detailed investigations into the magnetic ordering within this unique configuration. In this work, we examined the magnetic properties and magnetic structure of the half-sawtooth material $K_2Co_3(MoO_4)_3(OH)_2$, which contains S = 3/2 Co^{2+} ions. The structure is highly anisotropic with the magnetic easy axis coinciding with the long axis of the crystal, and the backbone of the sawtooth chain. The magnetic transition observed at T_N = 7 K is antiferromagnetic but the Weiss intercept is slightly positive (5.3(2) K) suggesting a ferromagnetic coupling in the structure. The effective magnetic moment is 4.8(3) μ_B which is well above the spin only value, but this is typical for Co^{2+} ions as they commonly

display spin orbit coupling. Isothermal magnetization exhibits a sharp field induced transition at 2 kOe, which can be resolved to a saturated state at a surprisingly low field of H = 2.5 kOe.

Neutron diffraction reveals an antiferromagnetic order as suggested by the magnetization data. The Co(1) ions forming the caps of the sawtooth structure are ferromagnetically coupled to each other along each chain, while the Co(2) ions in the backbone of the chain have canted vectors alternating along the chain approximately ferromagnetically coupled to each other, but antiferromagnetically related to the Co(2) ions within the chain. The half-sawtooth chains are antiferromagnetically coupled within the unit cell. This complex magnetic structure is consistent with other 1-D chains compounds. They can also show a very high sensitivity to external applied magnetic fields exhibiting multiple field induced transitions and this behavior is often a function of the re-orientation of the magnetic moment along the 1-D chain direction with the applied magnetic field. Such intricate relationships also imply more involved coupling relationships among the ions within and between the chains, and these values can be determined from subsequent inelastic neutron scattering experiments. The availability of suitable large single crystals will enable inelastic neutron scattering experiments in the future. As a result of the structural variation of the tetrahedral bridging group, we are able to systematically examine a wide range of magnetic properties of sawtooth and half-sawtooth chains.

Conflicts of Interest

There are no conflicts to declare.

Acknowledgements:

This research used resources at the Missouri University Research Reactor (MURR). This research used resources at the Spallation Neutron Source, which is a Department of Energy Office of Science User Facilities operated by the Oak Ridge National Laboratory. The work at University of Missouri and Clemson University was supported by awards from the NSF DMR – 2219129. Magnetic measurements taken at the University of Tennessee were supported by the DOE Early Career Program, Award DE-SC0021344.

References

[1] Tokura, Y.; Kawasaki, M.; Nagaosa, N. Emergent Functions of Quantum Materials. *Nature Phys.* **2017**, *13*, 1056–1068.
[2] Keimer, B., Moore, J. The Physics of Quantum Materials. *Nature Phys.* **2017**, *13*, 1045–1055.
[3] Giustino, F.; Lee, J. H.; Trier, F.; Bibes, M.; Winter, S. M.; Valentí, R.; Son, Y.; Taillefer, L.; Heil, C.; Figueroa, A. I.; Plaçais, B.; Wu, Q. S.; Yazyev, O. V.; Bakkers, E. P. A. M.; Nygård, J.; Forn-Díaz, P.; De Franceschi, S.; McIver, J. W.; Torres, L. E F. F.; Low, T.; Kumar, A.; Galceran, R.; Valenzuela, S. O.; Costache, M. V.; Manchon, A.; Kim, A.; Schleder, G. R.; Fazzio, A.; Roche, S. The 2021 Quantum Materials Roadmap. *J. Phys. Mater.* **2020**, *3*, 042006.
[4] Balents, L. Spin Liquids in Frustrated Magnets. *Nature* **2010**, *464*, 199−208,
[5] Head-Marsden, K.; Flick, J.; Ciccarino, C. J.; Narang, P.; Quantum Information and Algorithms for Correlated Quantum. *Chem. Rev.* **2021**, *121*, 3061−3120,
[6] Shaginyan, V. R.; Stephanovich, V. A.; Msezane, A. C.; Japaridze, G. S.; Clark, J. W.; Amusia, M. Y.; Kirichenko, E. V. Theoretical and Experimental Developments in Quantum Spin Liquid in Geometrically Frustrated Magnets: a Review. *J. Mater. Sci.* **2020**, *55*, 2257–2290.
[7] Scheie, A. O.; Ghioldi, E. A.; Xing, J.; Paddison, J. A. M.; Sherman, N. E.; Dupont, M.; Sanjeewa, L. D.; Lee, S.; Woods, A. J.; Abernathy, D.; Pajerowski, D. M.; Williams, T. J.; Zhang, S.-S.; Manuel, L. O.; Trumper, A. E.; Pemmaraju, C. D.; Sefat, A. S.; Parker, D. S.; Devereaux, T. P.; Movshovich, R.; Moore, J. E.; Batista C. D.; Tennant D. A.; *Nat. Phys.* **2023** https://doi.org/10.1038/s41567-023-02259-1.
[8] Taddei, K. M.; Garlea, V. O.; Samarakoon, A. M.; Sanjeewa, L. D.; Xing, J.; Heitmann, T. W.; Cruz, C.; Sefat, A. S.; Parker, D. Zig-Zag Magnetic Order and Potential Kitaev Interactions in the Spin-1 Honeycomb Lattice KNiAsO4. Phy. Rev. Res. 2023, 5, 013022.
[9] Han, T.-H.; Helton, J. S.; Chu, S.; Nocera, D. G.; Rodriguez-Rivera, J. A.; Broholm, C.; Lee, Y. S.; Fractionalized Excitations in the Spin-liquid State of a kagome-lattice Antiferromagnet *Nature* **2012**, *492*, 406–410.
[10] Stimpson, L. J. V.; Rodriguez, E. E.; Brown, C. M.; Stenning, G. B. G.; Jura, M.; Arnold, D. C.; Magnetic Ordering in a Frustrated Bow-tie Lattice. *J. Mater. Chem. C* **2018**, *6*, 4541–4548.
[11] Zhang, S.-Y.; Guo, W.-B.; Yang, M.; Tang, Y.-Y.; Cui, M.-Y.; Wang, N.-N.; He, Z.-Z.; A Frustrated Ferrimagnet $Cu_5(VO_4)_2(OH)_4$ with a 1/5 Magnetization Plateau on A New Spin-lattice of Alternating Triangular and Honeycomb Strips. *Dalton Trans.* **2015**, *44*, 20562–20567.

[12] Tang, Y.; Guo, W.; Xiang, H.; Zhang, S.; Yang, M.; Cui, M.; Wang, N.; He, Z.; Synthesis, Structure, and Magnetic Properties of $A_2Cu_5(TeO_3)(SO_4)_3(OH)_4$ (A = Na, K): The First Compounds with a 1D Kagomé Strip Lattice. *Inorg. Chem.* **2016**, *55*, 644−648.
[13] Garlea, V. O.; McGuire, M. A.; Sanjeewa, L. D.; Pajerowski, D. M.; Ye, F.; Kolis, J. W. The Magnetic Order of a Manganese Vanadate System with Two-dimensional Striped Triangular Lattice. *AIP Advances* **2018**, *8*, 101407.
[14] Sanjeewa, L. D.; Garlea, V. O.; Fishman, R. S.; Foroughian, M.; Yin, L.; Xing, J.; Parker, D. S.; Pellizzeri, T. M. S.; Sefat, A. S.; Kolis, J. W. Field Tunable Magnetic Transitions of $CsCo_2(MoO_4)_2(OH)$: A Triangular Chain Structure with a Frustrated Geometry. *Mater. Chem. Front.* **2023**, *7*, 1058–1071.
[15] Sanjeewa, L. D.; Garlea, V. O.; Taddei, K. M.; Yin, L.; Xing, J.; Fishman, R. S.; Parker, D. S.; Sefat, S. A. $NaCo_2(SeO_3)_2(OH)$: Competing Magnetic Ground States of a New Sawtooth Structure with $3d^7$ Co^{2+} ions. *Inorg. Chem. Front.* **2022**, *9*, 4329–4340.
[16] Garlea, O.; Sanjeewa, L. D.; McGuire, M.; Kumar, P.; Sulejmanovic, D.; He, J.; Hwu, S-J. Complex Magnetic Behavior of the Sawtooth Fe Chains in $Rb_2Fe_2O(AsO_4)_2$. *Physical Review B* **2014**, *89*, 014426.
[17] Liu, Y.; Sanjeewa, L. D.; Garlea, V. O.; Pellizzeri, T. M. S.; Kolis, J. W.; Sefat, A. S. Complex Magnetic Order in the Decorated Spin-chain System $Rb_2Mn_3(MoO_4)_3(OH)_2$. *Phys. Rev. B* **2020**, 101, 064423.
[18] Hagihala, M.; Hayashida, S.; Avdeev, M.; Manaka, H.; Kikuchi, H.; Masuda, T. Magnetic States of Coupled Spin Tubes with Frustrated Geometry in $CsCrF_4$. *npj Quantum Mater.* **2019**, *4*, 14.
[19] Acevedo, S.; Lamas, C. A.; Arlego, M.; Pujol, P.; Magnon Crystals and Magnetic Phases in a Kagome-stripe Antiferromagnet. *Phys. Rev. B* **2019**, *100*, 195145
[20] Chepiga, N.; Affleck, I.; Mila, F.; Floating, Critical, and Dimerized Phases in a Frustrated spin-3/2 Chain. *Phys. Rev. B 2020*, **101**, 174407.
[21] Garlea,V. O.; Sanjeewa, L. D.; McGuire, M. A.; Batista, C. D.; Samarakoon, A. M.; Graf, D.; Winn, B.; Ye, F.; Hoffmann, C.; Kolis, J. W. Exotic Magnetic Field-Induced Spin-Superstructures in a Mixed Honeycomb-Triangular Lattice System. *Phys. Rev. X* **201**9, *9*, 011038.
[22] Sanjeewa, L. D.; Garlea, V. O.; McGuire, M. A.; Xing, J.; Cao, H.; Kolis, J. W.; Sefat, A. S. Observation of Large Magnetic Anisotropy and Field-induced Magnetic State in $SrCo(VO_4)(OH)$: A Structure with Quasi One-Dimensional Magnetic Chain. *Inorg. Chem.* **2020**, *59*, 1029−1037.
[23] Sanjeewa, L. D.; Garlea, V. O.; McGuire, M. A.; Frontzek, M.; McMillen, C. D.; Fulle, K.; Kolis, J. W. Investigation of a Structural Phase Transition and Magnetic Structure of $Na_2BaFe(VO_4)_2$: A Triangular Magnetic Lattice with a Ferromagnetic Ground State. *Inorg. Chem.* **2017**, *56*, 14842−14849.
[24] McMillen, C. D.; Kolis, J. W. Hydrothermal Synthesis as a Route to Mineralogically-inspired Structures. *Dalton Trans.* **2016**, *45*, 2772−2784.
[25] Sanjeewa, L. D.; Ross, K. A.; Sarkis, C. L.; Nair, H. S.; McMillen, C. D.; Kolis, J. W. Single Crystals of Cubic Rare-Earth Pyrochlore Germanates: $RE_2Ge_2O_7$ (RE = Yb and Lu) Grown by a High-Temperature Hydrothermal Technique. *Inorg. Chem.* **2018**, *57*, 12456−12460.
[26] Kikuchi, H.; Fujii, Y.; Takahashi, D.; Azuma, M.; Shimakawa, Y.; Taniguchi, T.; Matsuo, A.; Kindo, K. Spin Gapped Behavior of a Frustrated Delta Chain Compound Euchroite. *J. Phys.: Conf. Ser.* **2011**, *320*, 012045.

[27] Yakubovich, O. V.; Shvanskaya, L. V.; Kiriukhina, G. V.; Simonov, S. V.; Volkov, A. S.; Dimitrova, O. V.; Glazkov, V. N.; Ignatenko, A. N.; Chung, S. H.; Koo, H.-J.; Whangbo, M.-H.; Vasiliev, A. N. $K_2Mn_3O(OH)(VO_4)(V_2O_7)$ with Sawtooth Chains of Multivalent Manganese Triangular Trimer Units: Magnetic Susceptibility Shrouding a Long-Range Antiferromagnetic Order of Ferromagnetic Triangles. *Inorg. Chem.* **2023**, *62*, 14180–14190.
[28] Pellizzeri, T. M. S.; McMillen, C. D.; Kolis, J. W. Alkali Transition-Metal Molybdates: A Stepwise Approach to Geometrically Frustrated Systems. *Chem.Eur.J.* **2020**, *26*, 597–600.
[29] Rosenkranz, S.; Osborn, R. Corelli: Efficient Single Crystal Diffraction with Elastic Discrimination. *PRAMANA - J. of Phys.* **2008**, *71*, 705–711.
[30] Coates, L.; Cao, H. B.; Chakoumakos, B. C.; Frontzek, M. D.; Hoffmann, C.; Kovalevsky, A. Y.; Liu, Y.; Meilleur, F.; dos Santos, A. M.; Myles, D. A. A.; Wang, X. P.; Ye F. A Suite-level Review of the Neutron Single Crystal Diffraction Instruments at Oak Ridge National Laboratory. *Rev. Sci. Instrum.* **2018**, *89*, 092802.
[31] Michels-Clark, T. M.; Savici,A. T.; Lynch, V. E.; Wang, X.; Chodkiewicz, M.; Weber, T.; Burgi, H.-B.; Hoffmann, C. M. Expanding Lorentz and Spectrum Corrections to Large Volumes of Reciprocal Space for Single-crystal Time-of-flight Neutron Diffraction. Corrigendum. *J. Appl. Cryst.* **2016**, *49*, 497–506
[32] Petříček, V.; Palatinus, L.; Plášil, J.; Dušek, M. Jana2020 – A New Version of the Crystallographic Computing System Jana. *Z. Kristallogr.* **2023**, *238*, 271–282.
[33] Rodríguez-Carvajal, J.; Recent Advances in Magnetic Structure Determination by Neutron Powder Diffraction. *Physica B: Condens.* **1993**, *192*, 55–69.
[34] Perez-Mato, J. M.; Gallego, S. V.; Tasci, E. S.; Elcoro, L.; de la Flor, G.; Aroyo, M. I. Symmetry-Based Computational Tools for Magnetic Crystallography. *Annu. Rev. Mater. Res.* 2015, 45, 217–248
[35] Aroyo, M. I.; Perez-Mato, J. M.; Capillas, C.; Kroumova, E.; Ivantchev, S.; Madariaga, G.; Kirov, A.; Wondratschek, H. Bilbao Crystallographic Server: I. Databases and Crystallographic Computing Programs. *Zeitschrift für Kristallographie - Crystalline Materials* 2006, 221, 15–27.
[36] Shanno, R. D. Revised Effective Ionic Radii and Systematic Studies of Interatomie Distances in Halides and Chaleogenides. *Acta Cryst.* **1976**, *A32*, 751–767.
[37] Sanjeewa, L. D.; Pellizzeri, T. M. S.; McMillen, C. D.; Taddei, K. M.; Heitmann, T.; Kaiser, K.; Kolis, J. W.; $SrNi(VO_4)(OH)$: The High-Temperature Hydrothermal Synthesis and Magnetic Properties of an adelite-descloizite-type Structure. *Crystals* **2022**, *12*, 1360.
[38] He, Z.; Fu, D.; Kyomen, T.; Taniyama, T.; Itoh, M.; Crystal Growth and Magnetic Properties of $BaCo_2V_2O_8$. *Chem. Mater.* **2005**, *17*, 2924–2926.
[39] Guo , H.; Zhao, L.; Baenitz, M.; Fabrèges, X.; Gukasov, A.; Sans, A. M.; Khomskii, D. I.; Tjeng, L. H.; Komarek, A. C.; Emergent 1/3 Magnetization Plateaus in Pyroxene $CoGeO_3$. *Phys. Rev. R* **2021**, *3*, L032037.
[40] He, Z.; Yamaura, J.-I.; Ueda, Y.; Cheng, W.; CoV_2O_6 Single Crystals Grown in a Closed Crucible: Unusual Magnetic Behaviors with Large Anisotropy and 1/3 Magnetization Plateau. *J. Am. Chem. Soc.* **2009**, *131*, 7554–7555.
[41] He, Z.; Guo, W.; Cui, M.; Tang, Y. Synthesis and Magnetic Properties of New Tellurate Compounds Na_4MTeO_6 (M = Co and Ni) with a Ferromagnetic Spin-chain Structure. *Dalton Trans.* **2017**, *46*, 5076−5081.
[42] Low, W. Paramagnetic and Optical Spectra of Divalent Cobalt in Cubic Crystalline Fields. *Phys. Rev. B* **1958**, *109*, 256.

[43] Lloret, F.; Julve, M.; Cano, J.; Ruiz-García, R.; Pardo, E.; Magnetic Properties of Six-coordinated High-Spin Cobalt(II) Complexes: Theoretical Background and its Application. *Inorganica Chimica Acta* **2008**, *361*, 3432–3445.

[44] Yuan, B.; Khait, I.; Shu, G. Chou, F. C.; Stone, M. B.; Clancy, J. P.; Paramekanti, A.; Kim, Y. Dirac Magnons in a Honeycomb Lattice Quantum XY Magnet $CoTiO_3$. *Phys. Rev. X.* **2020**, *10*, 011062.

[45] Cheng, J.; Tian, W.; Zhou, J.; Lynch, V. M.; Steinfink, H.; Manthiram A.; May, A. F.; Garlea,V. A.; Neuefeind, G. C.; Yan, J. Crystal and Magnetic Structures and Physical Properties of a New Pyroxene $NaMnGe_2O_6$ Synthesized under High Pressure. *J. Am. Chem. Soc.* **2013**, *135*, 2776−2786.

[46] Vasiliev, A. N.; Ignatchik, O. L.; Sokolov, A. N.; Hiroi, Z.; Isobe,M.; Ueda, Y. Long-range Magnetic Order in Quasi-one-dimensional Chromium-based (S = 3/2) pyroxene $(Li,Na)Cr(Si,Ge)_2O_6$. *Phys. Rev. B* **2005**, *72*, 012412.

[47] Pelissetto, A.; Vicari, E. Critical Phenomena and Renormalization-group Theory. Physics Reports **2002**, *368*, 549-727.

[48] Bera, A. K.; Lake, B.; Stein, W. D.; Zander, S.; Magnetic Correlations of the Quasi-one-Dimensional Half-integer Spin-chain Antiferromagnets $SrM_2V_2O_8$ (M = Co, Mn). *Phys. Rev. B* **2014**, *89*, 094402.